Mendeleev Communications

Mendeleev Commun., 2025, **35**, 393–395

$NaAlNb(PO_4)_3$ NASICON-type phosphate with the $Nb^{5+}/Nb^{4+}/Nb^{3+}$ multielectron redox activity on sodium intercalation

Ilia R. Cherkashchenko,*[a,b] Rodion V. Panin,[b] Alexander V. Babkin,[b] Daniil A. Novichkov,[b] Evgeny V. Antipov[a,b] and Nellie R. Khasanova[b]

[a] *Skolkovo Institute of Science and Technology, 143025 Moscow, Russian Federation. E-mail: ilyache.msu@gmail.com*

[b] *Department of Chemistry, M. V. Lomonosov Moscow State University, 119991 Moscow, Russian Federation*

DOI: 10.71267/mencom.7637

The NASICON-structured $NaAlNb(PO_4)_3$ phosphate was synthesized *via* Pechini sol–gel technique. Electrochemical measurements in sodium half-cells have disclosed that $NaAlNb(PO_4)_3$ can reversibly intercalate $2Na^+$ ions per formula unit owing to the $Nb^{5+}/Nb^{4+}/Nb^{3+}$ multielectron redox processes, which was confirmed by the Nb *K*-edge XANES measurements. Differential thermal calorimetry has revealed an excellent thermal stability of the sodiated $NaAlNb(PO_4)_3$/C electrode material up to the point of electrolyte decomposition.

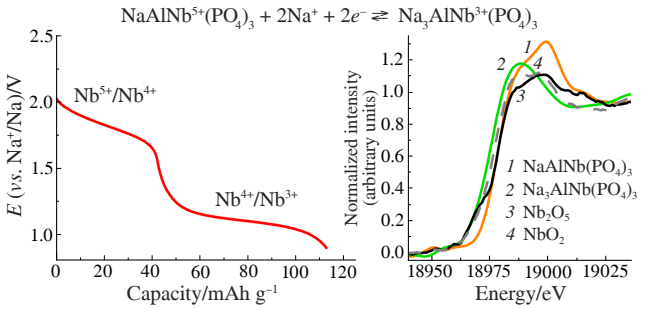

Keywords: NASICON-type phosphate, sodium-ion battery, niobium multielectron redox reaction, thermal stability, sol–gel synthesis.

The progress of modern society heavily relies on the development of renewable energy sources and the energy storage technologies improvement. Sodium-ion batteries (SIBs) are one of the most promising options for large-scale applications due to the abundance and low cost of sodium resources.[1,2] Despite numerous efforts to improve SIB anodes based on hard carbon, alloying and conversion[3] materials, safety concerns, such as lack of thermal stability[4] and sodium plating during high-rate cycling caused by their low operating potentials,[5] still remain significant flaws of these materials. That is why the development of safe anodes with suitable working potential (exceeding 1 V *vs.* Na^+/Na) is one of the main challenges for sodium-ion batteries technology.[6]

Recently, the NASICON-related niobium phosphates have been the subjects of extensive research.[7–10] Indeed, the utilization of niobium multielectron redox reactions occurring in the 1–2.3 V (*vs.* Na^+/Na) region, combined with the robust polyanionic framework, provides clear advantages for these compounds as promising candidates for next-generation anode materials in SIBs. However, most of these phases [$NaNbV(PO_4)_3$, $Na_{1.5}V_{0.5}Nb_{1.5}(PO_4)_3$ and $Nb_2(PO_4)_3$] contain low-valent d-metals and can only be prepared in an inert atmosphere, which hinders a scalable synthesis. Considering the $NaCrNb(PO_4)_3$ phosphate with the air stable Nb^{5+} and Cr^{3+} forms, the activation of the Cr^{3+}/Cr^{2+} redox couple on sodiation results in the appearance of Jan–Teller distortion of $Cr^{2+}O_6$ octahedron, restricting the rate capability of the material. From this perspective, the choice of Al^{3+} cation instead of Cr^{3+} or V^{3+} seems to be feasible due to its low weight, low cost, high stability and the ability to adapt to the NASICON structure.[11,12] Moreover, given the redox inertness of Al^{3+}, the possibility of activating the Nb^{3+}/Nb^{2+} couple within the NASICON framework upon $3Na^+$ uptake could be explored. Therefore, in this study we focused on the synthesis of the $NaAlNb(PO_4)_3$ phosphate and its investigation towards sodium intercalation.

$NaAlNb(PO_4)_3$ originally reported by Rangan and Gopalakrishnan,[13] has since been studied as sodium-ion conductor[14] and low thermal expansion material.[15] Only high temperature ceramic route has been used to prepare this compound, and no structural data have been presented for it. In this study, the NASICON-type phosphate, $NaAlNb(PO_4)_3$, was for the first time synthesized *via* Pechini sol–gel technique, which allowed us to decrease the annealing temperature (to 675 °C) and obtain a material suitable for electrochemical investigation.

X-ray powder diffraction (XRPD) data for $NaAlNb(PO_4)_3$ shown in Figure 1(*a*) were indexed in rhombohedral unit cell (space group $R\bar{3}c$, $Z = 6$), which is typical for the NASICON framework. The refined cell parameters $a = 8.4836(3)$ Å, $c = 21.8940(4)$ Å and $V = 1364.6(7)$ Å^3 matched well with previously published values.[14,15] The careful inspection of the XRPD pattern revealed several low-intensive reflections (<1%) arising from $NaNbO_3$ and $AlPO_4$ (73-1609 ICDD PDF-2 and 20-45 ICDD PDF-2, respectively). Rietveld refinement performed using the $NaCrNb(PO_4)_3$[8] as the initial structural model without any Al/Nb ordering was in the good agreement with the experimental profile [Figure 1(*a*)]. The reliable structural parameters and interatomic distances typical for all elements were achieved (see Online Supplementary Materials, Tables S1, S2). Electron microscopy data [Figure 1(*b*)] indicates that the sample consists of the micron-sized agglomerates formed by 60–100 nm egg-shape particles.

To improve the electron conductivity of $NaAlNb(PO_4)_3$ (Table S3) for further electrochemical measurements, we prepared carbon-coated $NaAlNb(PO_4)_3$/C samples using a polyacrylonitrile (PAN) pyrolysis technique,[16] and then single-walled carbon nanotubes (SWCNT) were added to the electrode composites ($NaAlNb(PO_4)_3$/C@SWCNT) for extended cycling. The cyclic voltammetry (CV) curve of the $NaAlNb(PO_4)_3$/C electrodes in the Na half-cell [Figure 2(*a*)] with 1M $NaPF_6$ at

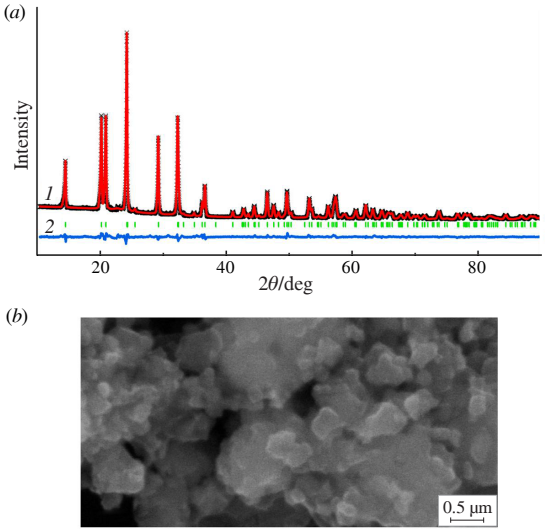

Figure 1 (*a*) XRD pattern of the $NaAlNb(PO_4)_3$ phase and its Rietveld refinement with observed data points (crosses), calculated pattern (*1*), difference curve (*2*) and Bragg positions (bars). (*b*) SEM image of the $NaAlNb(PO_4)_3$ sample.

ethylene carbonate (EC) : diethyl carbonate (DEC) volume ratio of 1 : 1 as the electrolyte shows two main peaks, which are apparently related to the redox transitions of Nb^{5+}/Nb^{4+} (~2 V *vs.* Na^+/Na) and the Nb^{4+}/Nb^{3+} (~1.1 V *vs.* Na^+/Na). A significant hysteresis (about 0.15–0.25 V) was observed in both cases, with the highest one for the Nb^{4+}/Nb^{3+} couple. It is noteworthy that the redox potentials of the corresponding niobium processes in the isostructural $NaMNb(PO_4)_3$ (M = V, Cr, Sc) niobium phosphates are lower at ~0.1 V.

A similar effect of the trivalent cation on the niobium redox potential has been previously reported for the $M_{0.5}Nb_{1.5}(PO_4)_3$ (M = Mn, Fe, Cr) NASICONs in a Li half-cell.[17] On the galvanostatic curve [Figure 2(*b*)], two successive inclined plateau-like regions were observed, and the specific capacity value (117 mAh g^{-1} at a C/10 rate) is quite close to the theoretical one (123 mAh g^{-1}), calculated for $2e^-$ transfer per formula unit. At a C/5 rate the capacity decreases to 95 mAh g^{-1}, and this loss occurs mainly within the low-voltage area (1–1.2 V). Galvanostatic cycling of the $NaAlNb(PO_4)_3$/C@SWCNT electrode showed the capacity retention to be 86% after 30 cycles at a C/10 rate [Figure 2(*c*)]. The material exhibited a high initial Coulombic efficiency (*ca.* 96%), which is typical for Nb-based polyanionic compounds.[7–10]

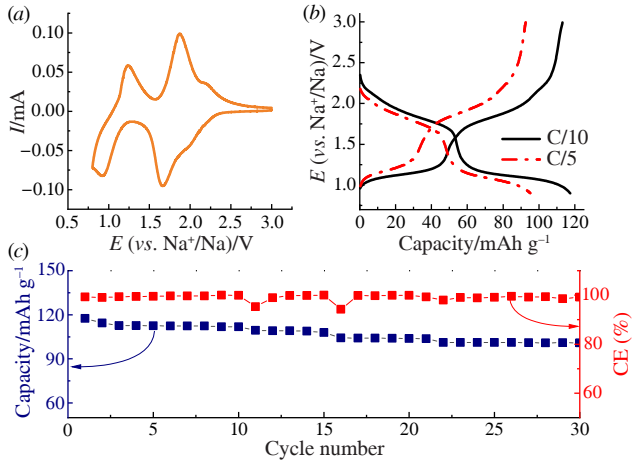

Figure 2 (*a*) The CV curve for the $NaAlNb(PO_4)_3$/C electrode, (*b*) the galvanostatic charge–discharge curves of the $NaAlNb(PO_4)_3$/C electrode at C/10 and C/5 rates and (*c*) cycling performance of the $NaAlNb(PO_4)_3$/C@SWCNT electrode at a C/10 rate in the voltage range of 0.8–3 V (*vs.* Na^+/Na).

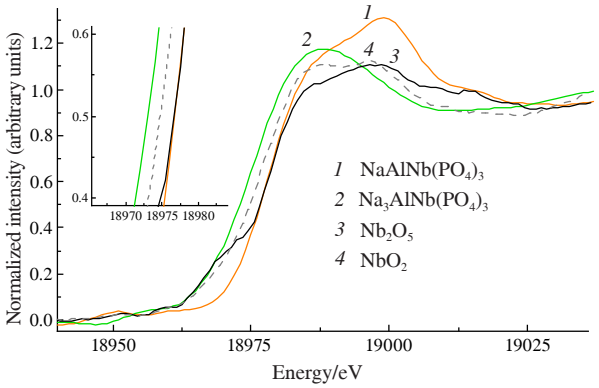

Figure 3 Normalized Nb *K*-egde XANES spectra of the pristine $NaAlNb(PO_4)_3$ (*1*) and sodiated $Na_3AlNb(PO_4)_3$ (*2*) phosphates compared with Nb_2O_5 (*3*) and NbO_2 (*4*) standards.

Ex situ Nb *K*-edge XANES measurements were performed to prove niobium reduction on sodiation. The resulting spectra (Figure 3) provide direct evidence of the multielectron $Nb^{5+}/Nb^{4+}/Nb^{3+}$ transfer. Thus, for the pristine sample, the Nb *K*-edge position is consistent with that of the Nb_2O_5 reference, while for the fully sodiated one (at 0.8 V *vs.* Na^+/Na), its spectrum exhibits a prominent shift to lower energies, leftward compared with the NbO_2 standard. Taking into account the electrochemical and XANES data, sodium intercalation into $NaAlNb(PO_4)_3$ can be represented by the following equation:

$$NaAlNb^{5+}(PO_4)_3 + 2Na^+ + 2e^- \rightleftharpoons Na_3AlNb^{3+}(PO_4)_3.$$

Thus, the electrochemical performance of $NaAlNb(PO_4)_3$ resembles that of $Na_3MnZr(PO_4)_3$[18] and $Na_4MnAl(PO_4)_3$,[19] the $Na_xMM'(PO_4)_3$ NASICON-type phosphates, where one metal (M) within the ($MM'O_6$) octahedral subsystem is electrochemically inactive, while the other one (M′) supports a $2e^-$ transition.

The thermal behavior of both 'dry' (without electrolyte) and 'wet' (with the electrolyte) sodiated $NaAlNb(PO_4)_3$-based electrode materials (Figure 4) is similar to that of the $NaCrNb(PO_4)_3$-based material without any significant exothermic peaks up to the electrolyte decomposition temperature (290 °C). Moreover, the heat flow from the 'wet' $NaAlNb(PO_4)_3$/C is almost six times less than in case of a 'wet' hard carbon anode (see Table S4).

According to our results, the $NaAlNb(PO_4)_3$ phosphate maintains a reversible intercalation of $2Na^+$ ions per formula unit due to the $Nb^{5+}/Nb^{4+}/Nb^{3+}$ redox transition. While the $NaMNb(PO_4)_3$ (M = Cr, V) phases exhibit the additional activation of the M^{3+}/M^{2+} couple, the $NaAlNb(PO_4)_3$ can be

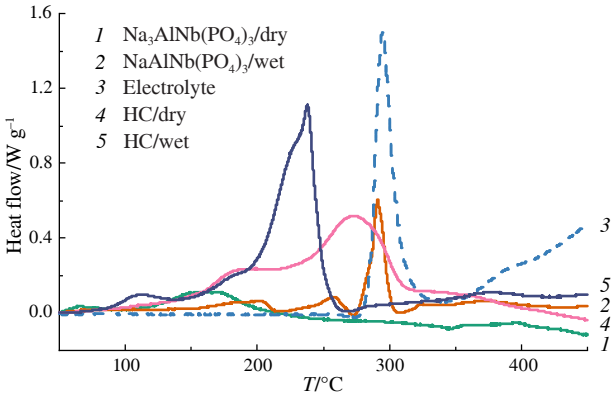

Figure 4 DSC curves for sodiated $NaAlNb(PO_4)_3$/C and hard carbon (HC) electrodes in 'dry' (without electrolyte) and 'wet' (with electrolyte) states.

considered as another example of an electrode material based solely on niobium redox processes similar to $NaScNb(PO_4)_3$[20] and $Nb_2(PO_4)_3$.[9] The shape of the galvanostatic curve for $NaAlNb(PO_4)_3$ allows one to assume that sodium intercalation into this phosphate occurs through a single-phase mechanism over the entire voltage range 0.8–3.0 V (*vs.* Na^+/Na), whereas, for example, in case of $NaCrNb(PO_4)_3$ a more complex process (with alternating single-phase and biphasic regions) has been observed.[8]

Thus, considering the close agreement between the experimental and calculated (for $2e^-$ transfer) specific capacities of $NaAlNb(PO_4)_3$ in the Na half-cell, we can conclude that there is an almost complete reversible transition of Nb^{5+} to Nb^{3+}, whereas for niobium oxide materials (Nb_2O_5, $TiNb_2O_7$, $TiNb_6O_{17}$, *etc.*) such deep reversible reduction has not been observed in either Li or Na half-cells.[21] In our research, we have not detected a further reduction of niobium towards Nb^{2+}. In fact, previous reports on the $Nb^{5+}\rightarrow Nb^{2+}$ reaction have revealed that extremely reducing conditions[22] or an immediate isolation of the arising Nb^{2+} in a zeolite 'cage' are required to preserve Nb^{2+} and prevent its rapid oxidation.[23] An extra stabilization of Nb^{2+} can be achieved through the formation of metallic clusters as a result of d–d overlapping between the neighboring niobium atoms.[24] However, in the NASICON framework the NbO_6 octahedra are isolated, and the Nb–Nb distance in the $NaAlNb(PO_4)_3$ structure exceeds 4.5 Å, thus hindering d–d interactions. Consequently, even if it would be possible to activate the Nb^{3+}/Nb^{2+} couple in the NASICON structure, the corresponding voltage would be too low, most likely outside the electrolyte stability window.

The authors acknowledge Russian Science Foundation (grant no. 23-13-00071) for supporting research work. The authors are grateful to Dr. Dmitriy Stolbov for providing SEM and EDX data, Dr. Sergey Istomin for his assisting with TG experiments and Dr. Ruslan Samigullin for his help in collecting DSC data.

Online Supplementary Materials

Supplementary data associated with this article can be found in the online version at doi: 10.71267/mencom.7637.

References

1 C. Vaalma, D. Buchholz, M. Weil and S. Passerini, *Nat. Rev. Mater.*, 2018, **3**, 18013; https://doi.org/10.1038/natrevmats.2018.13.
2 J. Deng, W.-B. Luo, S.-L. Chou, H.-K. Liu and S.-X. Dou, *Adv. Energy Mater.*, 2018, **8**, 1701428; https://doi.org/10.1002/aenm.201701428.
3 D. Yu. Gryzlov, T. L. Kulova, A. G. Nugmanova, A. M. Skundin and Y. O. Kudryashova, *Mendeleev Commun.*, 2024, **34**, 88; https://doi.org/10.1016/j.mencom.2024.01.026.
4 E. N. Abramova, Z. V. Bobyleva, O. A. Drozhzhin, A. M. Abakumov and E. V. Antipov, *Russ. Chem. Rev.*, 2024, **93**, RCR5100; https://doi.org/10.59761/RCR5100.
5 L. Fang, N. Bahlawane, W. Sun, H. Pan, B. B. Xu, M. Yan and Y. Jiang, *Small*, 2021, **17**, 2101137; https://doi.org/10.1002/smll.202101137.
6 Y.-S. Hu and Y. Lu, *ACS Energy Lett.*, 2019, **4**, 2689; https://doi.org/10.1021/acsenergylett.9b02190.
7 N. R. Khasanova, R. V. Panin, I. R. Cherkashchenko, M. V. Zakharkin, D. A. Novichkov and E. V. Antipov, *ACS Appl. Mater. Interfaces*, 2023, **15**, 30272; https://doi.org/10.1021/acsami.3c04576.
8 R. V. Panin, I. R. Cherkashchenko, V. V. Zaitseva, R. R. Samigullin, M. V. Zakharkin, D. A. Novichkov, A. V. Babkin, I. V. Mikheev, N. R. Khasanova and E. V. Antipov, *Chem. Mater.*, 2024, **36**, 6902; https://doi.org/10.1021/acs.chemmater.4c00933.
9 B. Patra, K. Kumar, D. Deb, S. Ghosh, G. Sai Gautam and P. Senguttuvan, *J. Mater. Chem. A*, 2023, **11**, 8173; https://doi.org/10.1039/D2TA05971A.
10 B. Patra, R. Hegde, A. Natarajan, D. Deb, D. Sachdeva, N. Ravishankar, K. Kumar, G. Sai Gautam and P. Senguttuvan, *Adv. Energy Mater.*, 2024, **14**, 2304091; https://doi.org/10.1002/aenm.202304091.
11 C. Wu, J. Tong, J. Gao, J. Li, X. Li, J. Zhu, M. Gu and W. Zhou, *ACS Appl. Energy Mater.*, 2021, **4**, 1120; https://doi.org/10.1021/acsaem.0c02203.
12 Q. Wang, C. Ling, J. Li, H. Gao, Z. Wang and H. Jin, *Chem. Eng. J.*, 2021, **425**, 130680; https://doi.org/10.1016/j.cej.2021.130680.
13 K. K. Rangan and J. Gopalakrishnan, *Inorg. Chem.*, 1994, **34**, 1969; https://doi.org/10.1021/ic00111a055.
14 A. R. Shaikhlislamova, A. Yu. Goryainov and A. B. Yaroslavtsev, *Inorg. Mater.*, 2010, **46**, 896; https://doi.org/10.1134/S0020168510080170.
15 A. I. Orlova, A. K. Koryttzeva, Ye. V. Lipatova, M. V. Zharinova, I. G. Trubach, Yu. V. Evseeva, N. V. Buchirina, G. N. Kazantsev, S. G. Samoilov and A. I. Beskrovny, *J. Mater. Sci.*, 2005, **40**, 2741; https://doi.org/10.1007/s10853-005-2120-7.
16 E. E. Nazarov, O. A. Tyablikov, V. A. Nikitina, E. V. Antipov and S. S. Fedotov, *Appl. Nano*, 2023, **4**, 25; https://doi.org/10.3390/applnano4010002.
17 M. Manickam, K. Minato and K. Takata, *J. Electrochem. Soc.*, 2003, **150**, A1085; https://doi.org/10.1149/1.1589019.
18 H. Gao, I. D. Seymour, S. Xin, L. Xue, G. Henkelman and J. B. Goodenough, *J. Am. Chem. Soc.*, 2018, **140**, 18192; https://doi.org/10.1149/1.1589019.
19 Y. Zheng, J. Liu, D. Huang, H. Chen and X. Xou, *Surf. Interfaces*, 2022, **32**, 102151; https://doi.org/10.1016/j.surfin.2022.102151.
20 L. Znaidi, S. Launay and M. Quarton, *Solid State Ionics*, 1997, **93**, 273; https://doi.org/10.1016/S0167-2738(96)00558-9.
21 Q. Deng, Y. Fu, C. Zhu and Y. Yu, *Small*, 2019, **15**, 1804884; https://doi.org/10.1002/smll.201804884.
22 C. Cartier, T. Hammouda, M. Boyet, O. Mathon, D. Testemale and B. N. Moine, *Am. Mineral.*, 2015, **100**, 2152; https://doi.org/10.2138/am-2015-5330.
23 H. S. Lim, N. H. Heo and K. Seff, *Microporous Mesoporous Mater.*, 2020, **303**, 110265; https://doi.org/10.1016/j.micromeso.2020.110265.
24 E. V. Anokhina, M. W. Essig, C. S. Day and A. Lachgar, *J. Am. Chem. Soc.*, 1999, **121**, 6827; https://doi.org/10.1021/ja990759e.

Received: 3rd October 2024; Com. 24/7637